Magnetite (Fe3O4) and nickel ferrite (NiFe2O4) zeta potential measurements at high temperature: Part II – Results, study of the influence of temperature, boron concentration and lithium concentration on the zeta potential

Chloé Cherpin, Derek Lister, Frédéric Dacquait, Sarita Weerakul, Lihui Liu

To cite this version:

Chloé Cherpin, Derek Lister, Frédéric Dacquait, Sarita Weerakul, Lihui Liu. Magnetite (Fe3O4) and nickel ferrite (NiFe2O4) zeta potential measurements at high temperature: Part II – Results, study of the influence of temperature, boron concentration and lithium concentration on the zeta potential. Colloids and Surfaces A: Physicochemical and Engineering Aspects, 2022, 647, pp.129030. 10.1016/j.colsurfa.2022.129030 . cea-04574515

HAL Id: cea-04574515

https://cea.hal.science/cea-04574515v1

Submitted on 22 Jul 2024

Magnetite (Fe_3O_4) and nickel ferrite ($NiFe_2O_4$) zeta potential measurements at high temperature: Part II – Results, study of the influence of temperature, boron concentration and lithium concentration on the zeta potential.

Dr. Chloé Cherpin[1,2,*] chloe.cherpin@cea.fr
Dr. Derek Lister[2] dlister@unb.ca
Frédéric Dacquait[1] frederic.dacquait@cea.fr
Dr. Sarita Weerakul[2] sarita.weerakul@unb.ca
Dr. Lihui Liu[2] lihui@unb.ca

[1]CEA, DES, IRESNE, DTN, Cadarache
F-13108 Saint-Paul-Lez-Durance, France

[2]Chemical Engineering Department,
University of New Brunswick
P.O. Box 4400, Fredericton, N.B., Canada, E3B 5A3

*Corresponding author:
E-mail address: chloe.cherpin@cea.fr

Abstract

Predicting the deposition of typical corrosion products (CPs) particles formed in the primary system of pressurized water reactors (PWRs) is important for system integrity and the radioprotection of nuclear workers. Such corrosion products foul heat transfer surfaces, promote localized corrosion and, when made radioactive in the reactor core, transport throughout the coolant system and give rise to radiation fields around components. Accurately predicting CPs' propensity to transport and deposit around the system entails knowing their zeta potentials, quantities that until now have been unavailable. The zeta potentials of magnetite and nickel ferrite particles between 20 °C and 240 °C have been measured in the chemical conditions representative of an operating cycle of the primary system of PWRs. The measurements were performed via the streaming potential method as described in a previous paper – Part I. The measured values increased with temperature but decreased with increasing concentrations of boron and lithium. They are suitable for predicting radiation field growth around components of a typical PWR system.

Keywords

High temperature zeta potential – streaming potential – boron / lithium chemistry – magnetite – nickel ferrite – primary system – pressurized water reactor

1. Introduction

In pressurized water reactors (PWRs), the formation, transport and deposition of activated corrosion products (ACPs) carrying radionuclides such as ^{58}Co, ^{60}Co or ^{110m}Ag generate radiation fields that contribute about 85% to the dose absorbed by workers during operation and maintenance [1]. Understanding the mechanisms underlying this activity transport in the reactor coolant system is important for minimizing worker doses.

As a result of the corrosion of the metals (stainless steels and nickel based alloys) of components in contact with the high-temperature primary coolant water, a well-known double layer oxide structure [2–6] is formed. The inner oxide, close to the base metal, is enriched in chromium and has a very fine-grained structure based on spinel chromite. The outer oxide is formed of coarse crystals, up to a few micrometres in size, with an inverse spinel ferrite structure and contains slabs of nickel hydroxide [3–5].

Transported ACPs in the primary coolant exist either in ionic or particulate form, coming from either the dissolution or the mechanical degradation of the oxides. Hence, the composition of particles is often approximated to the composition of the outer oxide on the metal components. Particulate oxides range in size from several micrometres to sub-micrometre, according to the operating phase of the reactor [7]. Studies of the distributions, by mass and by number, of particle size [8–11] have noted that a significant proportion of corrosion products is found within a size range inferior to 3 µm, which encompasses colloidal size (generally taken to be 1 µm or below). In terms of radioactive distribution, however, particles larger than 5 µm are the most significant [7,12]. It should be noted that plants have their own unique operating history and such studies of particle size distribution cannot generally be applied to more than one plant.

Due to the wide range of particle size in the primary coolant, it is important to take into account both inertial effects (predominant for large particle deposition, say for particles with a size superior to several micrometres) and surface effects (predominant for colloids) in a comprehensive deposition model.

Predicting the deposition of particles traditionally relies on the determination of the particle deposition coefficient, K_D [13]. As deposition is often modelled as consisting of two independent steps in series, transport and attachment, K_D may be expressed as:

$$\frac{1}{K_D} = \frac{1}{K_T} + \frac{1}{K_A} (equation\ 1)$$

where K_T and K_A are respectively the transport and attachment coefficients.

The attachment step for colloidal particles depends on the attractive London-Van-der-Waals force and the electrical double layer force, either repulsive or attractive; these are decisive in the deposition process. The prediction of the deposition of colloidal particles on a surface is usually solved by using the well-known DLVO (Derjaguin, Landau, Vervey and Overbeek) [14] theory. This theory relies on the evolution of the interaction energy either between two particles, to predict aggregation, or between a particle and a surface, to predict deposition. In practice, the forces $\vec{F}$ influencing particles derive from a potential ϕ:

$$\vec{F} = -\vec{\nabla}\phi\ (equation\ 2)$$

The total interaction potential ϕ_T can be expressed as:

$$\phi_T = \phi_A + \phi_R \; (equation\ 3)$$

where ϕ_A and ϕ_R are respectively the potentials arising from attractive and repulsive forces. In the classic DLVO theory, the attractive forces consist of the Van der Waals forces and the electrical double layer force (if the particle and the surface have surface charges of opposite sign); likewise, the repulsive forces consist of the electrical double layer force (if the particle and the surface have surface charges of same sign) and the Born repulsive force (due to the repulsion between the atomic orbitals of the particle and of the surface).

From the DLVO theory, the evolution of the interaction potential between the particle and the surface with the particle-surface distance determines whether an energy barrier exists and its value, the comparison between the kinetic energy of the particle with this barrier will in turn determine if deposition occurs or not. Clearly, in order to apply the theory, values of the fundamental potentials of the particles and the surface – the zeta potential values – are required.

A few studies have aimed at the measurement of zeta potentials or at the measurement of the point/pH of zero charge (PZC) (pH for which the zeta potential value is zero) of various oxides at the temperatures of the primary system of PWRs. Barale [15,16], using mass titration, managed to obtain values of zeta potential of magnetite, nickel ferrite and cobalt ferrite up to 70 °C and was the only one to publish measurements of the PZC of typical oxides of the primary system up to 320 °C; however, the chemical conditions were not fully representative of those of the primary system, since they employed background ions in salts such as LiCl and KCl.

To determine the zeta potential values of typical oxides of the primary system, especially nickel ferrite and magnetite, a test section using the streaming potential method [17] was custom-built and connected to a high-temperature and high-pressure recirculating loop in the laboratory.

This paper describes the measurements performed in chemical conditions representative of the primary coolant of PWRs at temperatures ranging from 20 °C to 240 °C. The results are presented, and the influence on the zeta potential of the temperature of the system and the boron and lithium concentrations are discussed. The set of values forms the basis of a transport/deposition model for colloidal particles.

2. Materials and methods

2.1 Particles

Magnetite (Fe_3O_4) and nickel ferrite ($NiFe_2O_4$) are of interest as being representative of particulate corrosion products of the primary system. Commercial magnetite was used in the experiments but the nickel ferrite was synthesized to the desired stoichiometry using an optimized solid-state method, described elsewhere [18], that heats ingredient oxides in an evacuated 10 cm long quartz vial (see Figure 1). Synthesized nickel ferrite particles are shown in the SEM picture in Figure 1, obtained with a Jeol 6400 microscope. The individual particles ranged in size from about 0.3 µm to 1.3 µm and appeared to have agglomerates or clumps between 2 µm and 7 µm. Magnetite powder was purchased from Sigma-Aldrich with a purity of 95 % and a particle size stated as below 5 µm. As shown in the SEM in Figure 1, the actual particle size range was below about 0.3 µm.

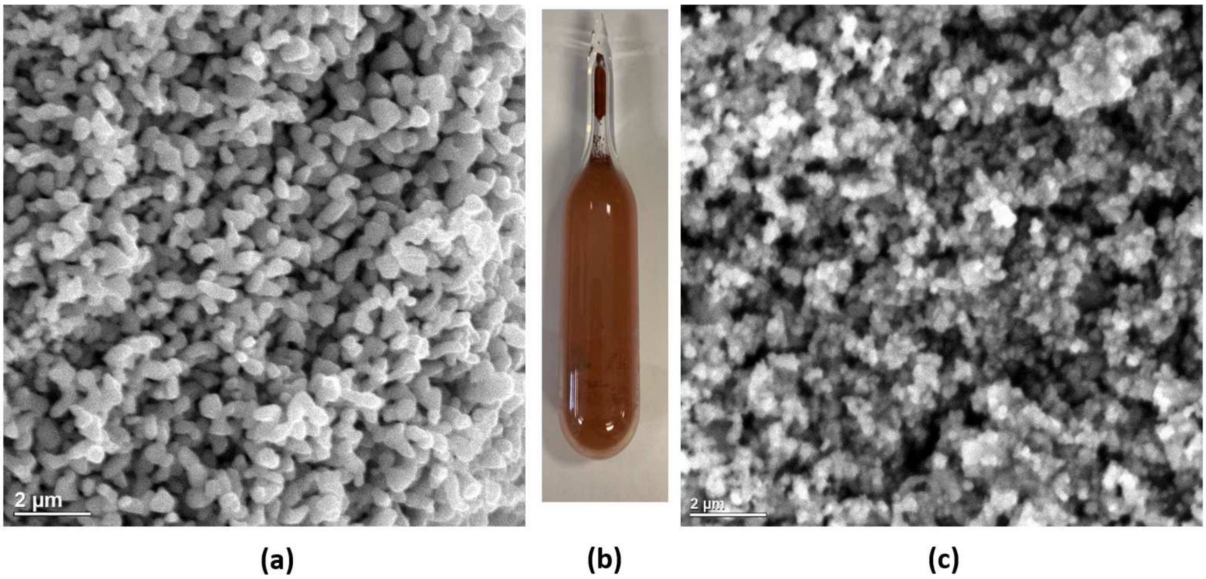

Figure 1. (a) SEM picture of synthesized nickel-ferrite (b) Quartz-vial used for the solid state-synthesis (c) SEM picture of commercial magnetite. (one and a half page width)

2.2 Streaming potential test section and high-temperature and –pressure recirculating loop

A test section was custom-built [17] for installation in a high-temperature experimental water loop to determine the zeta potential of the nickel ferrite and magnetite at different temperatures and boron/lithium co-ordinations pertinent to PWR coolant conditions. The test section contains a column, electrically insulated from the loop material, that holds the sample powder between porous ceramic membranes, allowing coolant to flow through the powder as a packed bed. Electrodes at each end of the column allow the streaming potential to be measured.

The protocol used to prepare and run blank measurements is described elsewhere [17]. Once the powder is packed in the column between the two membranes, the test section is installed in a bypass in the loop. With the loop conditions adjusted to the desired temperature and chemical conditioning, the test section is valved-in and the pressure drop across it is measured as well as the streaming potential and the electrical resistance across the packed powder [17].

Using the equation from Jayaweera [19] for a cylindrical tube, the zeta potential value can be determined:

$$\frac{\Delta V}{\Delta P} = \frac{\varepsilon_0 \varepsilon_r R r^2 \zeta}{4 \eta L} \quad (equation\ 4)$$

where ΔV is the streaming potential, ΔP is the pressure drop across the test section due to the packed bed of particles, ε_0 the permittivity of free space, ε_r the relative permittivity, R the electrical resistance, r the radius of the column, η the dynamic viscosity, L the length of the packed bed and ζ the zeta potential.

2.3 Experimental conditions

As the goal is to determine the zeta potential values of magnetite and nickel ferrite in the chemical conditions of the primary system of PWRs, twelve different boron/lithium co-ordinations representative of a high-lithium chemistry regime comprised twelve experimental runs (see Figure 2). Note that throughout the paper the concentrations are expressed in ppm, parts per million, which corresponds to mg/kg. The concentrations of lithium were measured with KHP titrations and the concentrations of boron with the curcumin colorimetric-extraction method [20].

For each condition, the zeta potential was measured for magnetite and nickel ferrite between 20 and 200 °C. For the last condition ([B]=1800 ppm and [Li]=3.5 ppm), the temperature was at its highest – 240 °C.

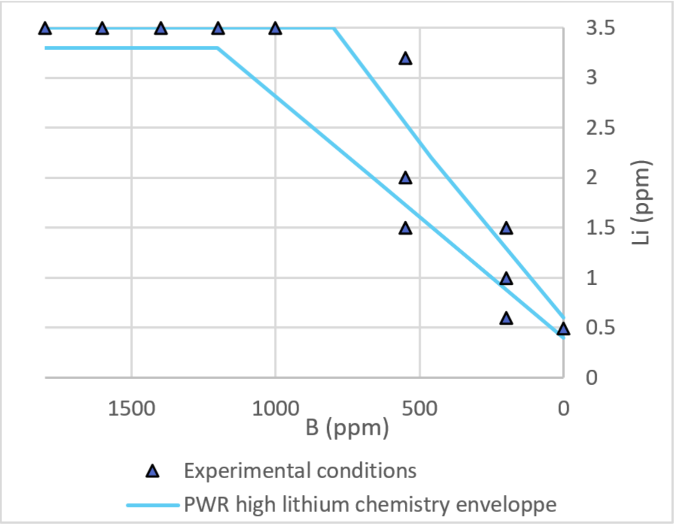

Figure 2. Boron/lithium co-ordinations imposed in the system and PWR high-lithium chemistry envelope. (small column size)

3. Results and discussion

3.1 Zeta potential values

Prior to each measurement involving a powder, blank measurements of pressure drop were performed on the empty column first. The blank values were subtracted from the subsequent measurements with the powder in place. Blank measurements of streaming potential and resistance proved negligible [17]. For a zeta potential measurement, the pressure drop and the potential values across the column filled with 0.5 g of powder were measured and their values were averaged over a measuring time of approximately 10 min. This was followed by a measurement of the electrical resistance of the column. The measurement protocol is described elsewhere [17].

For the same conditions, different trials led to the same evolution of the average streaming potential as a function of the pressure drop across the packed oxide column [17]. Using a linear regression between the averaged streaming potential and the pressure drop, the slope of the line is extracted and the zeta potential value calculated using the resistance measurement and the values of the viscosity and relative permittivity of water at the corresponding temperature in Jayaweera’s formula (equation 4) [19]. Thus, the value of the zeta potential of the packed powder is determined.

Table 1, and Table 3 present the values of zeta potential (in mV) of magnetite and nickel ferrite obtained for the different boron/lithium co-ordinations for temperatures between 20 and 200 °C and

Table 2 presents the zeta potentials values of magnetite obtained between 200 and 240 °C for [B]=1800 ppm and [Li]=3.5 ppm.

B/Li co-ordination	20 °C	50 °C	100 °C	150 °C	200 °C
0/0.5	-6.7 ±0.5	-6.2 ±0.5	-3.6 ±0.3	-1.2 ±0.1	-0.9 ±0.1
200/0.6	-4.4 ±0.3	-2.9 ±0.2	-2.0 ±0.2	0.0 ±0.1	1.1 ±0.1
200/1.0	-5.2 ±0.4	-3.2 ±0.2	-2.4 ±0.2	-1.4 ±0.1	0.5 ±0.1
200/1.5	-5.4 ±0.4	-4.4 ±0.3	-3.5 ±0.3	-2.5 ±0.2	-0.9 ±0.1
550/1.5	-5.1 ±0.4	-4.8 ±0.4	-3.8 ±0.3	-2.8 ±0.2	0.2 ±0.1
550/2.0	-6.3 ±0.5	-5.2 ±0.3	-4.1 ±0.2	-3.2 ±0.2	0.0 ±0.1
550/3.2	-6.4 ±0.4	-5.5 ±0.4	-4.8 ±0.4	-4.0 ±0.3	-0.8 ±0.1
1000/3.5	-4.7 ±0.3	-3.9 ±0.3	-3.1 ±0.2	-1.6 ±0.1	1.0 ±0.1
1200/3.5	-7.1 ±0.5	-5.9 ±0.4	-4.0 ±0.3	-2.4 ±0.2	0.1 ±0.1
1400/3.5	-7.9 ±0.6	-6.4 ±0.5	-5.6 ±0.4	-4.0 ±0.3	-1.6 ±0.1
1600/3.5	-8.5 ±0.8	-7.7 ±0.6	-5.9 ±0.4	-4.5 ±0.3	-1.5 ±0.1
1800/3.5	-9.3 ±0.7	-8.8 ±0.7	-7.8 ±0.6	-6.4 ±0.5	-2.6 ±0.2

Table 1. Values of zeta potential (mV) obtained for magnetite for the different boron/lithium (expressed as B/Li) co-ordinations for temperatures ranging from 20 °C to 200 °C.

Temperature (°C)	Zeta potential value (mV)
210	-2.5 ±0.2
220	-1.9 ±0.1
230	-1.6 ±0.2
240	-1.3 ±0.1

Table 2. Values of zeta potential of magnetite for temperatures ranging from 210 °C to 240 °C ([B]=1800 ppm and [Li]=3.5 ppm)

B/Li co-ordination	20 °C	50 °C	100 °C	150 °C	200 °C
0/0.5	-9.9 ±0.7	-5.5 ±0.4	-5.2 ±0.4	-0.6 ±0.1	-0.3 ±0.1
200/0.6	-8.0 ±0.6	-5.0 ±0.5	-3.2 ±0.4	0.9 ±0.1	3.5 ±0.3
200/1.0	-10.5 ±0.3	-6.7 ±0.2	-4.0 ±0.2	-1.4 ±0.1	-0.5 ±0.1
200/1.5	-14.2 ±1.0	-12.0 ±1.0	-10.0 ±0.9	-8.5 ±0.6	-5.6 ±0.4
550/1.5	-4.6 ±0.3	-3.5 ±0.2	-2.0 ±0.3	-0.5 ±0.4	0.7 ±0.1
550/2.0	-6.1 ±0.2	-4.9 ±0.1	-3.7 ±0.4	-1.9 ±0.3	-0.1 ±0.1
550/3.2	-8.7 ±0.6	-7.5 ±0.6	-5.6 ±0.4	-3.7 ±0.4	-2.1 ±0.2
1000/3.5	-6.5 ±1.3	-5.2 ±1.3	-2.9 ±0.6	-1.6 ±0.6	1.5 ±0.6
1200/3.5	-7.0 ±1.3	-5.9 ±0.9	-3.7 ±0.8	-1.8 ±0.5	0.8 ±0.4
1400/3.5	-7.9 ±0.5	-6.5 ±0.5	-4.5 ±0.7	-2.5 ±0.8	0.0 ±0.8
1600/3.5	-9.3 ±0.7	-8 ±0.4	-6.4 ±0.5	-4.0 ±0.6	-2.3 ±0.2

1800/3.5	-13.0 ±0.9	-12.0 ±1.0	-9.1 ±0.7	-6.1 ±0.5	-4.2 ±0.3

Table 3. Values of zeta potential (mV) obtained for nickel ferrite for the different boron/lithium co-ordinations for temperatures ranging from 20 °C to 200 °C.

The uncertainties corresponding to the zeta potential values were computed by propagation of uncertainty in Equation 4. For temperatures, as type K thermocouples were used, an uncertainty of ±2.2 °C was considered. For pressure measurements, as the sensors were calibrated prior to the experimental campaign, no measurement error was reported. The uncertainties concerning electrical resistance measurement and potential measurement were computed through standard deviation. The measurement error concerning the length and radius of the packed bed was taken equal to 0.5 mm.

Barale [15] obtained zeta potential values of magnetite and nickel ferrite at 20 °C in conditions where almost the same concentration of boron as ours was used (550 ppm in this study and 500 ppm in Barale's). In order to study the effect of Li on the zeta potential, Barale used various concentrations of LiCl and used a solution of KCl as reference, as K$^+$ and Cl$^-$ are indifferent toward the surface of oxides. The pH was adjusted by addition of HCl, KOH or LiOH. The comparison is thus difficult since, in this work, lithium was used at various concentrations to reproduce the co-ordinations representative of the functioning cycle of a PWR. Table 4 gives a comparison of the results obtained in this study and in Barale's with KCl and LiCl at the same pH at 25 °C

		This study	Barale [15]	
	pH (25 °C)	20 °C [B]=550 ppm +Li	25 °C [B]=500 ppm [KCl]=10^{-4} mol/kg	25 °C [B]=500 ppm [LiCl]=10^{-4} mol/kg
NiFe$_2$O$_4$	6.9	-4.6 ±0.3 mV	-2 mV	10 mV
	7.2	-6.1 ±0.2 mV	-5 mV	2 mV
	7.4	-8.7 ±0.7 mV	-9 mV	-2 mV
Fe$_3$O$_4$	6.9	-5.1 ±0.4 mV	-18 mV	-13 mV
	7.2	-6.3 ±0.5 mV	-25 mV	-20 mV
	7.4	-6.4 ±0.4 mV	-33 mV	-25 mV

Table 4. Comparison of zeta potential values extracted from Barale with those obtained in this work for nickel ferrite and magnetite particles.

As shown in Table 4, the background ions used by Barale considerably influence the zeta potential values, as the zeta potential measured with LiCl is greater than with KCl, for both magnetite and nickel ferrite, considerably so for nickel ferrite. For nickel ferrite, the results obtained by Barale with KCl are in good agreement with those found in this study. For magnetite, however, the differences are large with either KCl or LiCl.

The difference in zeta potential values between this study and Barale's may also be linked to the nature of the particles used for the measurements. Indeed, the choice of the preparation conditions of the sample influences the value of the zeta potential, as shown by Jayaweera [21]. For two differently-prepared samples of magnetite, a difference in 2.3 mV for the value of PZC was observed, one sample seemingly retaining more negative charges than the other. The magnetite used in Barale's study was purchased from Alfa Aesar while ours was from Sigma Aldrich, which may explain the differences in zeta potential measurements.

3.2 Influence of the temperature on the zeta potential value

The zeta potential for magnetite and nickel ferrite was determined for temperatures up to 200 °C for different boron/lithium chemistries (see Figure 3 and Figure 4). For both magnetite and nickel ferrite, the zeta potential increases with the temperature. For some boron/lithium co-ordinations, the zeta potential can even become positive above 150 °C.

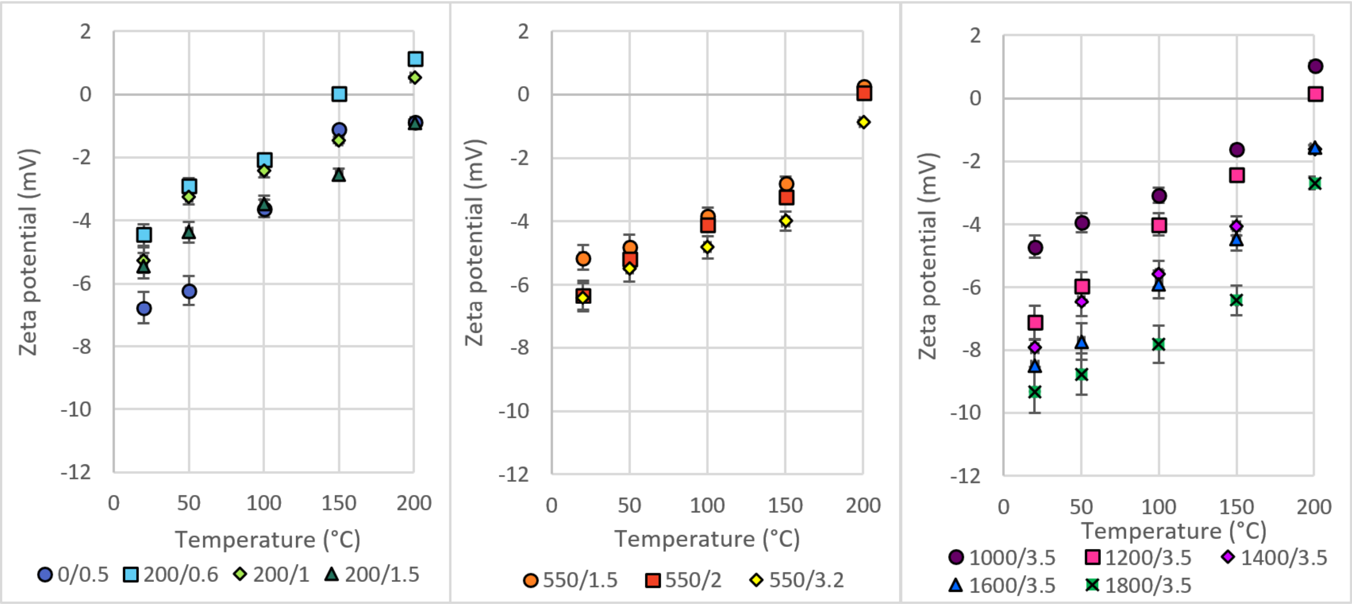

Figure 3. Evolution with temperature of the zeta potential of magnetite for different boron/lithium co-ordinations. (full page width)

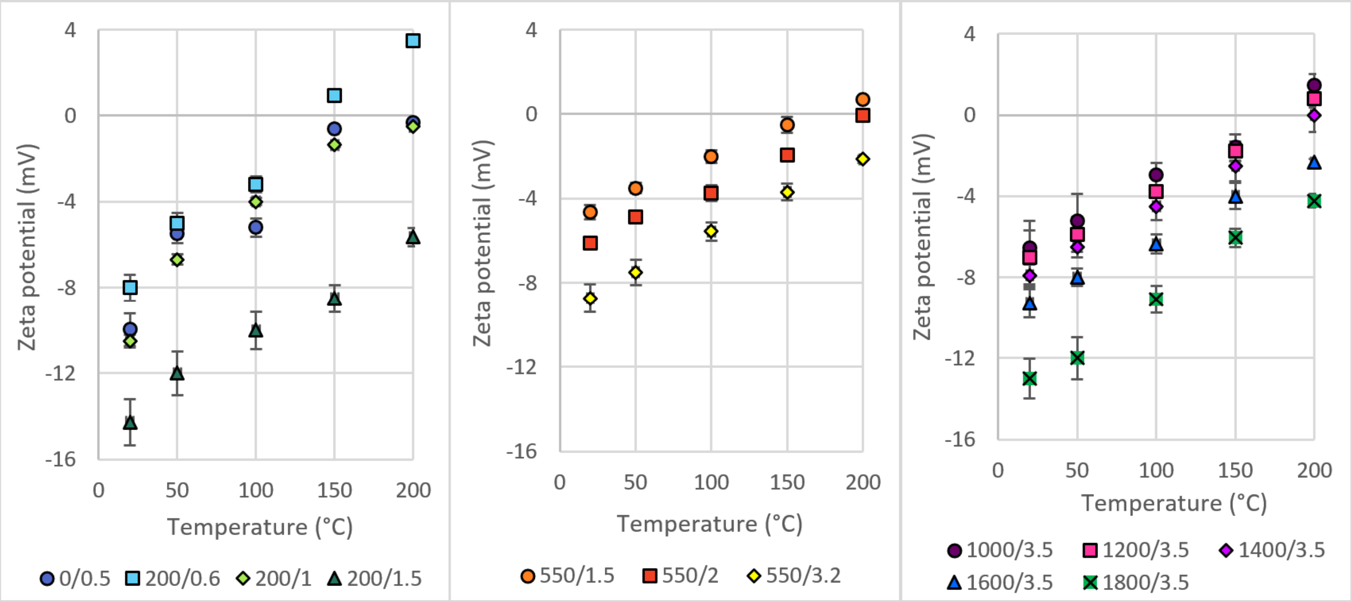

Figure 4. Evolution with temperature of the zeta potential of nickel ferrite for different boron/lithium co-ordinations. (full page width)

Figure 5 shows the evolution of the zeta potential of magnetite between 20 °C and 240 °C, where [B]=1800 ppm and [Li]=3.5 ppm (a co-ordination commonly employed in plants at the start of cycle). The value increases fairly linearly for temperatures above 200 °C; at and below 150 °C the linearity is less clear, but the linear regression through all the data with the R^2 value of 0.983 is not unreasonable. The data also demonstrate that the streaming potential technique produces reliable measurements, since they are in satisfactory agreement for the two different runs at temperatures at and below 200 °C. Points above 200 °C were obtained from a single run.

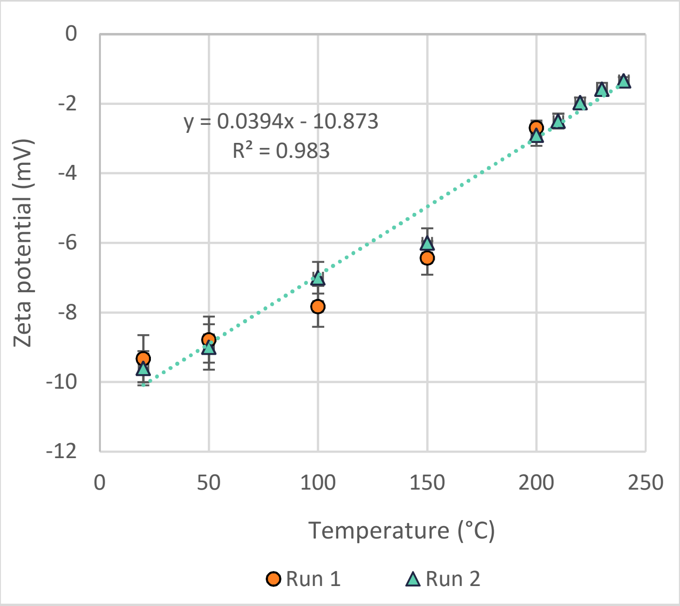

Figure 5. Evolution of the zeta potential value of magnetite with temperature and the linear regression through all data ([B]=1800 ppm [Li]=3.5 ppm). (small column size)

The test section arrangement in the high-temperature loop would not allow experiments to continue at temperatures above 240 °C; however, if it is assumed that the linear correlation is valid for higher temperatures, the zeta potential values (for a fixed boron/lithium coordination) can be predicted (see Figure 5). From the extrapolation, the zeta potential of magnetite becomes positive above 280 °C.

The influence of temperature on the value of the zeta potential is significant. The temperature doesn't explicitly appear in the formula to determine the zeta potential value but is implicitly taken into account in the viscosity, η, and relative permittivity, ε_r, of the coolant. It also directly influences the electrical resistance of the column (see, for example, Figure 6). For every chemical condition and for both the magnetite and nickel ferrite columns, the measured electrical resistance decreases with increasing temperature.

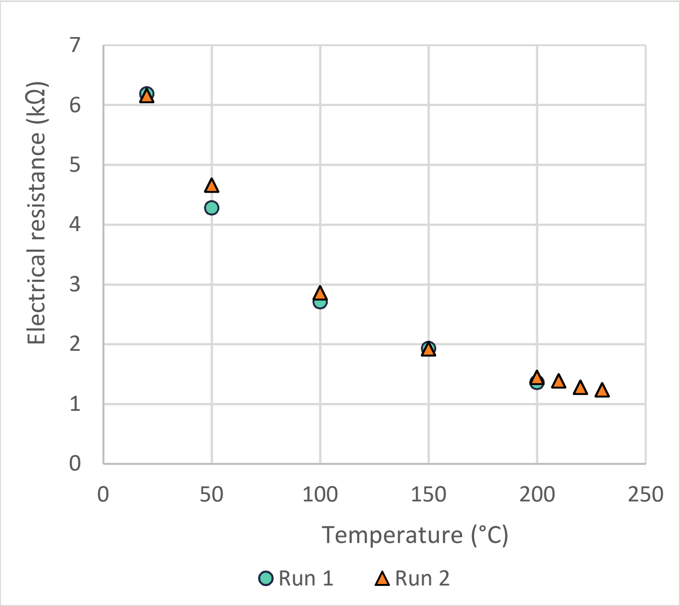

Figure 6. Influence of the temperature on the electrical resistance of the magnetite column for duplicate runs ([B]=1800 ppm and [Li]=3.5 ppm) (small column size)

Furthermore, the temperature influences the pressure drop over the empty test section $\Delta P_{empty\ test\ section}$ and therefore the pressure drop across the packed bed [17], as:

$$\Delta P_{packed\ test\ section} = \Delta P_{packed\ bed} + \Delta P_{empty\ test\ section}\ (equation\ 5)$$

Note that the $\Delta P_{empty\ test\ section}$ was determined at the beginning of each run and subtracted from the $\Delta P_{packed\ test\ section}$ to give the desired $\Delta P_{packed\ bed}$ during the run. Typically, the empty test section value (mainly contributed by the pressure drop across the membranes) was 60% of the packed test section value.

In addition, the measured streaming potential also depends on the temperature as shown in Figure 7, where the dotted lines are linear regressions.

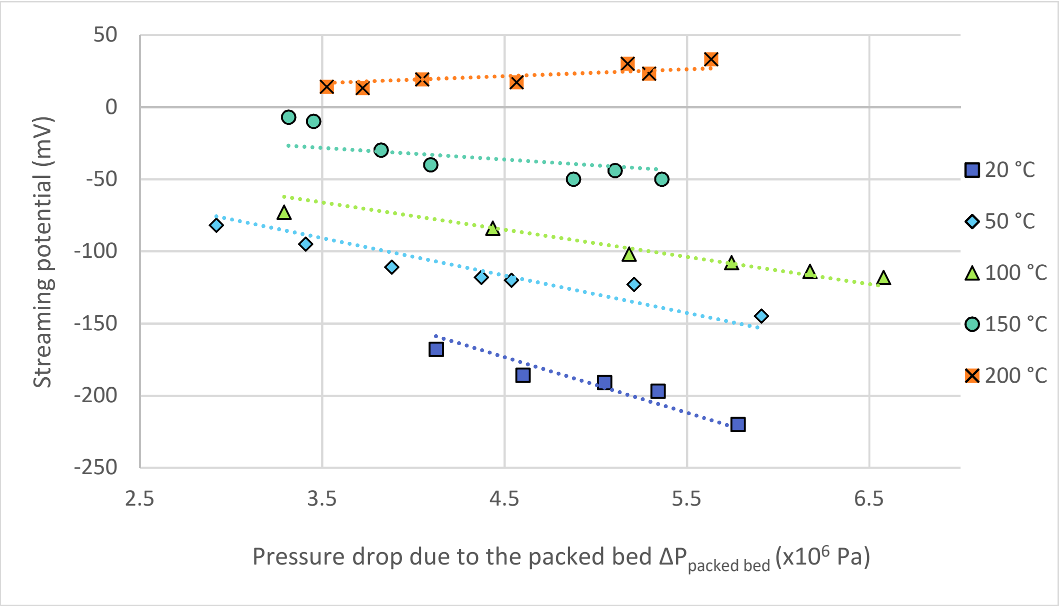

Figure 7. Streaming potential as a function of the pressure drop across the packed bed for a column packed with 0.5 g of magnetite between 20 °C and 200 °C for [B]=200 ppm and [Li]=1.5 ppm. (One and a half page width)

To summarize, with increasing temperature, the streaming potential increases. While the pressure drop and electrical resistance decrease; the consolidated result is an increase of the zeta potential value with increasing temperature.

3.3 Boric acid and lithium hydroxide chemistry

In this work, the influence of the boron/lithium co-ordination on the zeta potential is studied. The aqueous chemistry of boric acid is complex, with polyborates forming at the conditions of a PWR fuelling cycle. The early high-temperature (up to 300°C) study by Mesmer et al. [22] of boric acid in dilute solutions with potassium chloride indicated the formation of the orthoborate ion:

$$B(OH)_3 + OH^- \rightleftharpoons B(OH)_4^- \quad (equation\ 6)$$

The formation of diborate $B_2(OH)_7^-$ and triborate $B_3(OH)_{10}^-$ occurred in boric acid solutions up to 0.6 mol/kg (~7,000 ppm as [B]) by successive $B(OH)_3$ additions:

$$B(OH)_4^- + B(OH)_3 \rightarrow B_2(OH)_7^- \ (equation\ 7)$$

$$B_2(OH)_7^- + B(OH)_3 \rightarrow B_3(OH)_{10}^- \ (equation\ 8)$$

along with minor amounts of higher polymeric species. The possibility of structures such as an oxygen bridge and ring respectively for the diborate and triborate molecules was postulated from thermodynamic considerations.

The recent study by Sasidharanpillai et al. [23] indicated that at least ten different borate and polyborate species exist in boric acid solutions at different conditions. The following equilibria were characterised:

$$B(OH)_3 + OH^- \rightleftharpoons B(OH)_4^- \ (equation\ 9)$$

$$2B(OH)_3 + OH^- \rightleftharpoons B_2(OH)_7^- \ (equation\ 10)$$

$$3B(OH)_3 + OH^- \rightleftharpoons B_3O_3(OH)_4^- + 3H_2O \ (equation\ 11)$$

$$4B(OH)_3 + 2OH^- \rightleftharpoons B_4O_5(OH)_4^{2-} + 5H_2O \ (equation\ 12)$$

$$5B(OH)_3 + OH^- \rightleftharpoons B_5O_6(OH)_4^- + 6H_2O \ (equation\ 13)$$

We note that with an added base such as lithium hydroxide, the equilibrium:

$$Li^+ + OH^- \rightleftharpoons LiOH \ (equation\ 14)$$

leads to a salt such as lithium orthoborate:

$$Li^+ + B(OH)_4^- \rightleftharpoons LiB(OH)_4 \ (equation\ 15)$$

The overall scheme is completed with the dissociation of water:

$$H_2O \rightleftharpoons H^+ + OH^- \ (equation\ 16)$$

Ferguson et al. [24] concluded that in dilute solutions at temperatures above 200 °C the diborate is the major anionic species followed by triborate (20-30% of total anions) and borate (at 10-15%), whereas below 200 °C, triborate in the major ionic specie.

It is clear that at different temperatures and concentrations of boric acid and lithium hydroxide, the anions available for adsorption on colloidal oxides and modification of the zeta potential are varied. Steric considerations suggest that the hydroxide ion should be favoured followed by orthoborate. A full study of the systems under our experimental conditions, which would involve techniques for aqueous chemistry measurements at high temperature, is outside the scope of this paper. It is appropriate, however, to consider the overall effects of the coolant chemistries imposed.

3.4 Influence of the pH on the zeta potential value

The pH dependence of the zeta potential of any system is defined through the Point of Zero Charge (PZC), defined above as the pH where the concentration of positively charged and negatively charged sites on a surface are equal. Therefore, if the pH is below the PZC, the zeta potential is positive. If the pH is equal to the PZC, by definition the zeta potential is equal to zero. Otherwise, the zeta potential becomes negative. Thus, by definition the zeta potential value decreases with increasing pH.

For each boron/lithium coordination, the pH at the temperature corresponding to the experiment was calculated using PhreeqCEA, a chemistry code and database adapted from the geochemistry code PhreeqC developed by the US Geological Survey for PWR conditions [25] (see Figure 8).

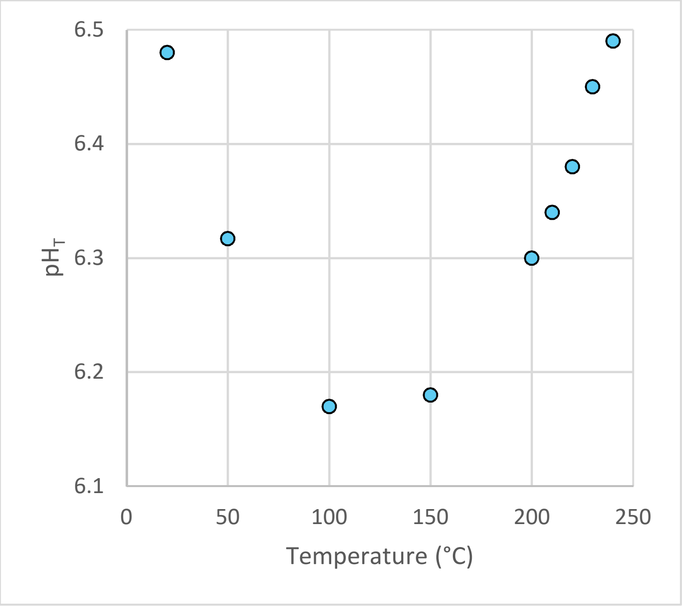

Figure 8. Evolution of the pH_T with the temperature for [B]=1800 ppm and [Li]=3.5 ppm. (small column size)

For each pH at experimental temperature, pH_T, the corresponding zeta potentials for solutions with the same boron or lithium concentration are plotted to obtain Figure 9 and Figure 10. From these figures, the evolution of the zeta potential with the pH for a fixed B/Li co-ordination can be followed. For low concentrations of boron (up to 550 ppm), for both magnetite and nickel ferrite, as the pH increases the zeta potential decreases. A zeta potential decrease means that more anions than cations are accumulating within the layer of ions close to the particle. This is related to the increasing concentration of OH^- and $B(OH)_4^-$ ions in the solution. For higher boron concentrations (between 1000 and 1800 ppm), the effect of the pH_T on the zeta potential value is less clear as the pH_T evolution with temperature has an inverse-bell-shaped curve, as shown in Figure 8 for example.

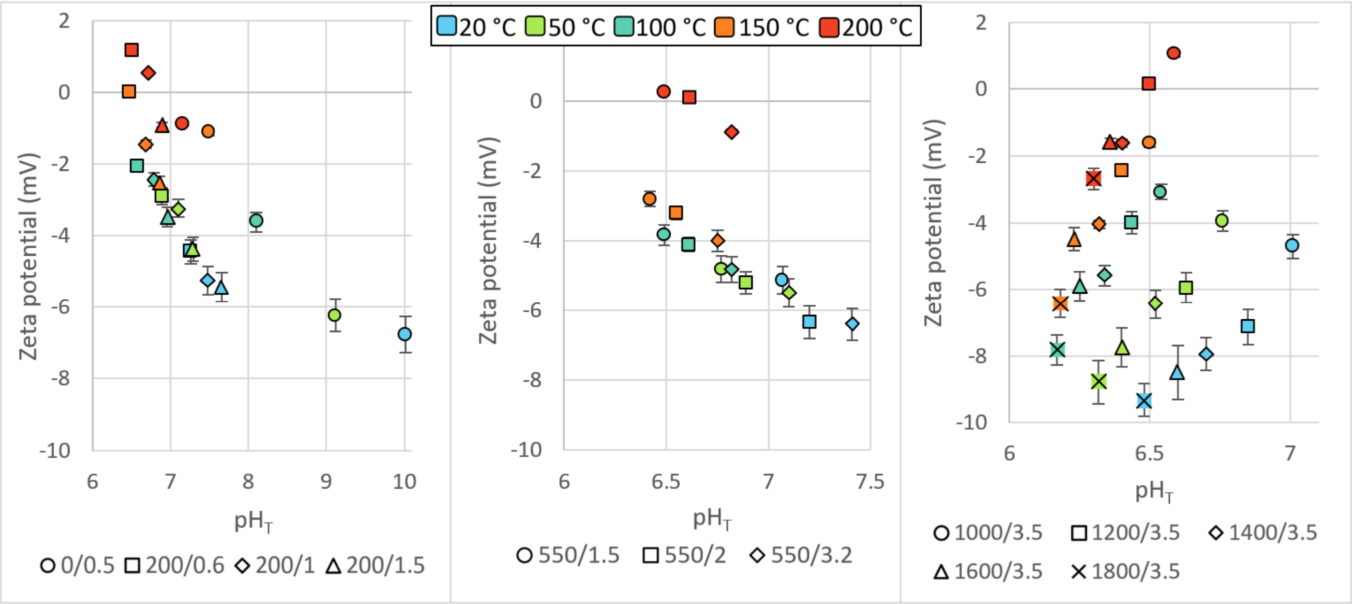

Figure 9. Evolution of zeta potential with pH_T of systems with a given boron/lithium coordination (written as B/Li) for a magnetite packed column. (full page width)

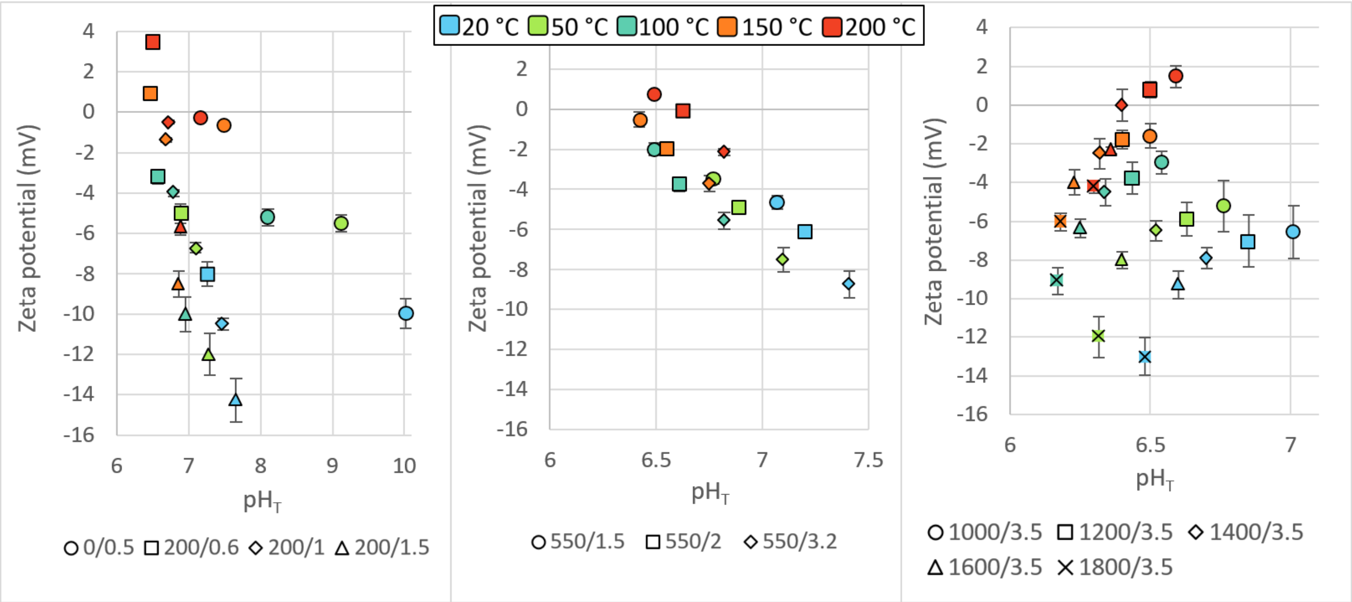

Figure 10. Evolution of zeta potential with pH_T of systems with a given boron/lithium coordination (written as B/Li) for a nickel ferrite packed column. (full page width)

Barale [15] measured with mass titration the value of PZC of magnetite and nickel ferrite for different temperatures with [KCl]=10^{-2} mol/kg. The measured PZC values were always lower than the pH_T. For the temperatures of 25 °C, 50 °C and 90 °C, the zeta potential values of magnetite and nickel ferrite measured in this study are always negative when the pH_T is above the PZC. In the absence of more data for comparison, this assessment demonstrates a level of agreement between this study's zeta potential values and Barale's.

In this study, however, as the pH of the system is governed by the concentrations of lithium hydroxide and boric acid in the loop reacting as controlled by the equilibria introduced above, only a small range of pH can be studied. The pH_T calculated for PWR operating temperature has an even smaller range than the measured range at ambient temperature (see Table 5).

B (ppm)	Li (ppm)	pH_{EPRI} [26] (25°C)	$pH_{PhreeqCEA}$ (300 °C)
0	0,5	9.85	7.18
200	0,6	6.9	6.95
200	1	7.1	7.17
200	1,5	7.27	7.34
550	1,5	6.72	7.06
550	2	6.85	7.18
550	3,2	7.06	7.38
1000	3,5	6.65	7.21
1200	3,5	6.48	7.14
1400	3,5	6.33	7.07
1600	3,5	6.19	7.02
1800	3,5	6.07	6.97

Table 5. Values of the pH at 25 °C from the EPRI and the PhreeqCEA values for 300 °C at the corresponding B/Li co-ordinations

It is more revealing to link the zeta potential to the separate effects of lithium and boron ions. Accordingly, the influence on the zeta potential value of lithium hydroxide (for a fixed concentration of boric acid) and, conversely, of boric acid (for a fixed concentration of lithium hydroxide) is examined.

3.5 Influence of lithium hydroxyde concentration

Figure 11 and Figure 12, respectively for magnetite and nickel ferrite, show the influence of the lithium concentration on the value of the zeta potential for a fixed concentration of boron. The same trend is observed for both oxides: an increasing concentration of lithium leads to a decreasing value of zeta potential.

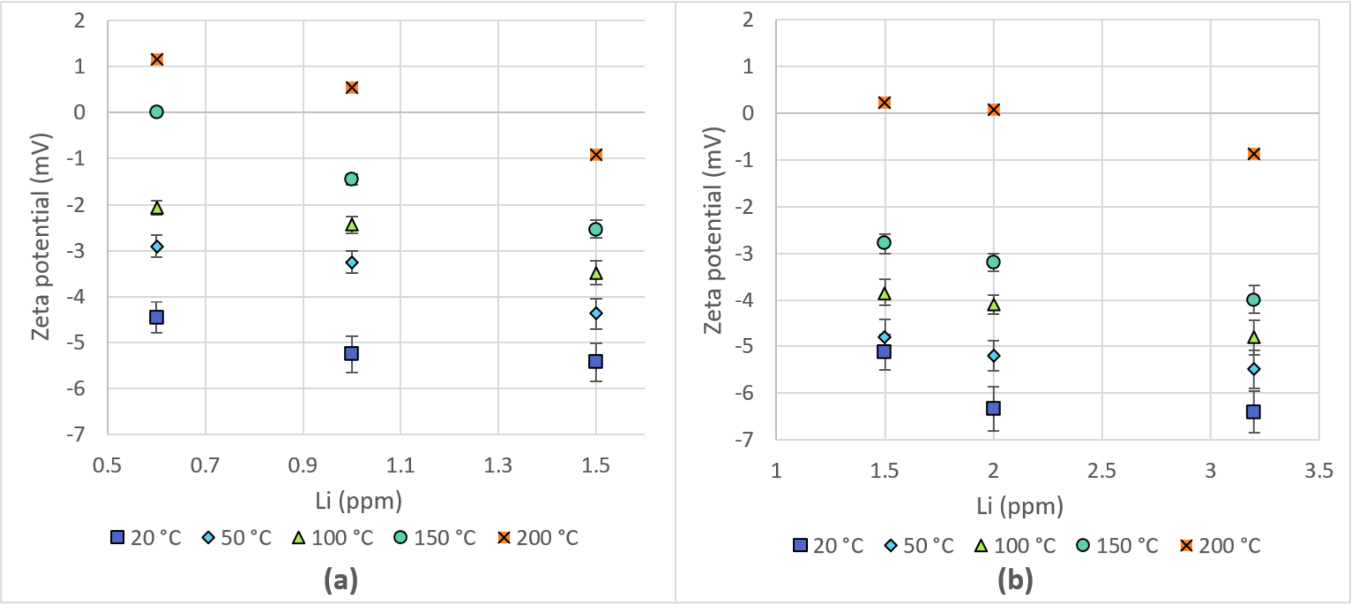

Figure 11. Effect of the lithium concentration on the zeta potential of magnetite for a fixed concentration of boron of (a) 200 ppm and (b) 550 ppm. (full page width).

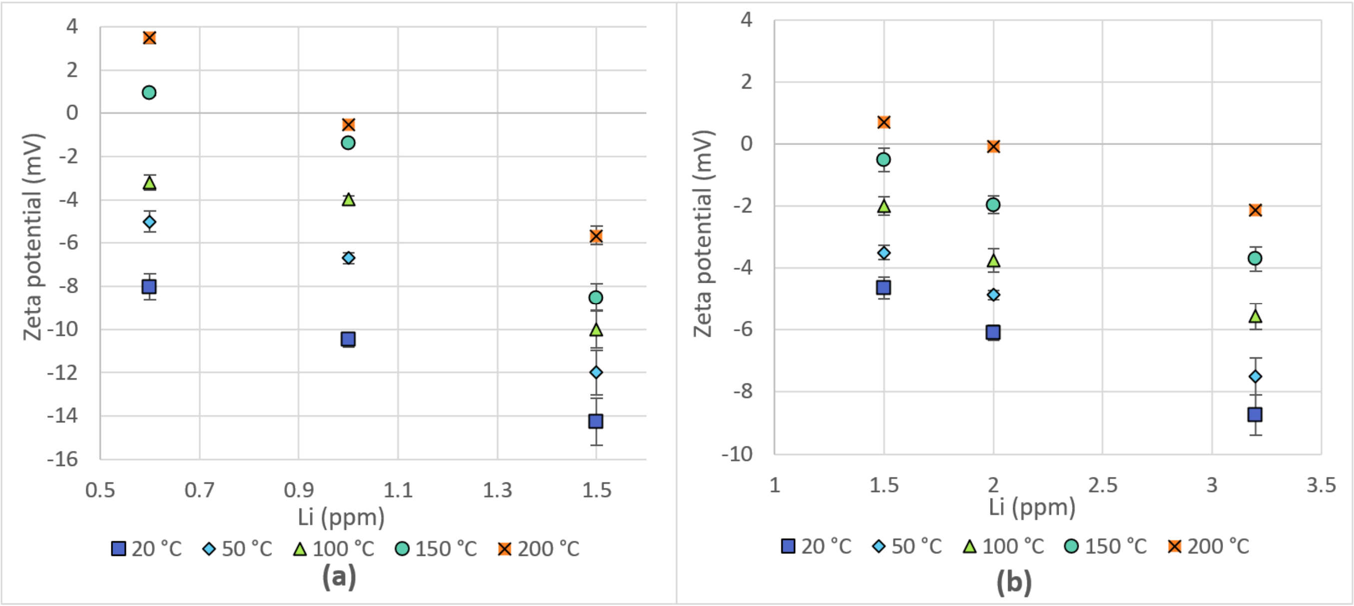

Figure 12. Effect of the lithium concentration on the zeta potential of nickel ferrite for a fixed concentration of boron of (a) 200 ppm and (b) 550 ppm. (full page width).

Concerning the effect of lithium ions themselves on the zeta potential, Barale [15,16] suggested that due to their positive charge, high charge density and hydration state, lithium ions cannot access the

Stern layer and therefore do not come close to the charged surface. The introduction of lithium hydroxide, however, leads to the introduction of hydroxide ions which will predominate in the Helmholtz layer and thus lead to a decrease of the zeta potential value.

Overall, the introduction of lithium hydroxide leads to the decrease of the zeta potential value due to the increase of the pH and the predominance of hydroxide ions as the lithium ions are indifferent toward the surface of the particles.

3.6 Influence of boric acid on the zeta potential value

Figure 13 shows that an increasing boric acid concentration leads to a decrease of the zeta potential value for magnetite and nickel ferrite. This is attributed to the adsorption of borates by magnetite and nickel ferrite as shown by Deshon and Frattini [27] and confirmed by studied conducted by EPRI [6].

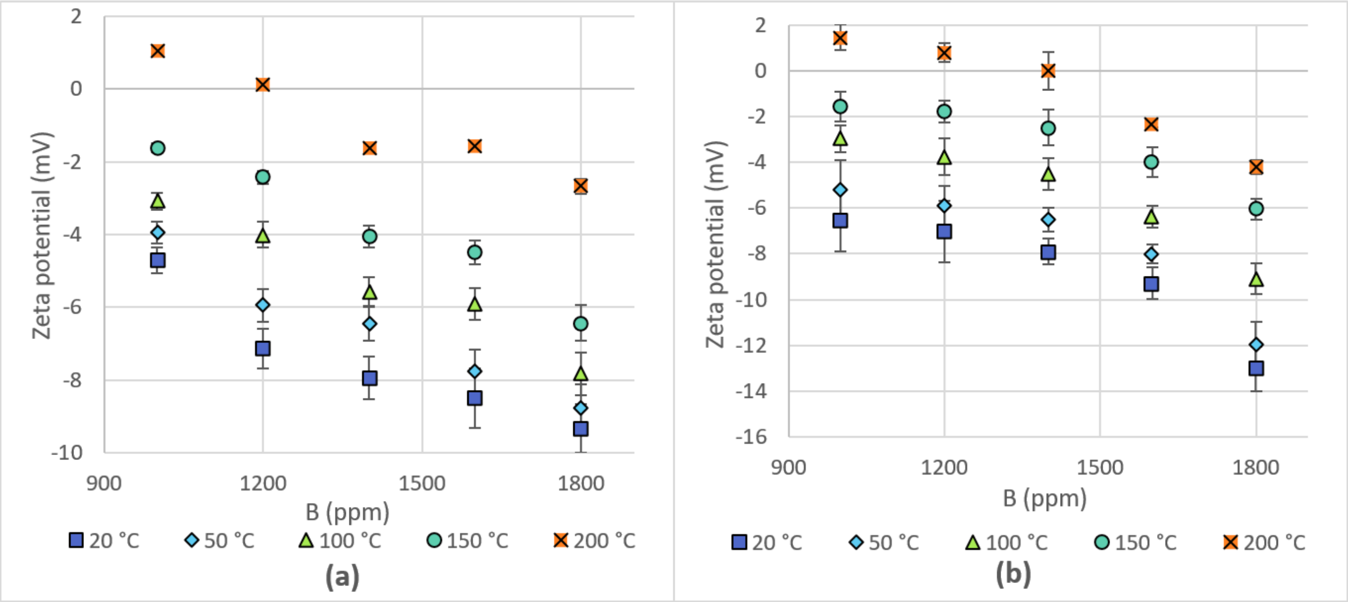

Figure 13. Effect of the boron concentration on the zeta potential of (a) magnetite and (b) nickel ferrite for [Li]=3.5 ppm. (full page width).

Indeed, when boron (as boric acid) is adsorbed on the surface of a solid (M-OH in Figure 14, inspired by Peak [28]), a ligand is exchanged and a negative co-ordination sphere is formed. The chemisorption of borates creates a tightly-bound layer of negative charges next to the surface of the solid phase. As a consequence, the first layer around the surface will be predominantly positive ions, quite strongly attracted to the surface. The following layers of charged species will form the diffuse layer, that will be swept away during the streaming potential measurement. As the zeta potential sign is related to the charges found between the surface and shear plane, the observed decrease of the zeta potential value with an increase in the borate concentration means that the amount of negatively charged species in the tightly bound ionic layers increases with the boron concentration.

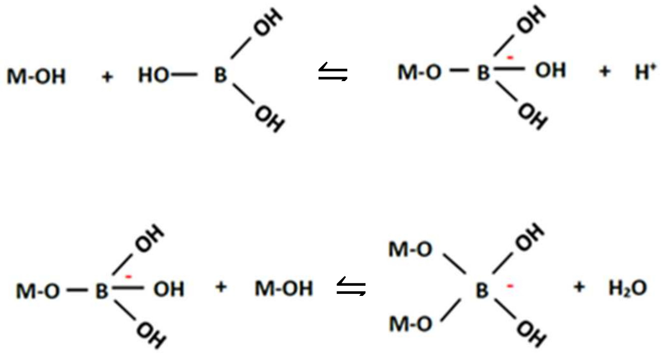

Figure 14. Possible reactions for the adsorption of boric acid on a surface. (small column size)

As shown in Figure 13, for a fixed boron concentration, an increasing temperature increases the zeta potential value, which is confirmed by results from Deshon and Frattini [27]. Indeed, as temperature increases the adsorption of borate species decreases, giving an increase in the zeta potential value. Also, a temperature increase has an impact on the pH (see Figure 8), as above 100 °C, the pH increases, the zeta potential is expected to decrease. As a zeta potential increase is observed when temperature increases, the predominant effect of borate adsorption is thus put forward.

For each temperature, the difference between the zeta potential measured for a concentration in boron of 1800 ppm and the zeta potential for a concentration of 1000 ppm was determined for magnetite and nickel ferrite (see Figure 15). From this graph, magnetite shows bigger differences than nickel ferrite for temperatures up to 200 °C, when the two oxides have similar values. For magnetite, the effect of boric acid on the zeta potential value decreases with temperature, whereas for nickel ferrite, there are no evident effect from temperature on the zeta potential difference.

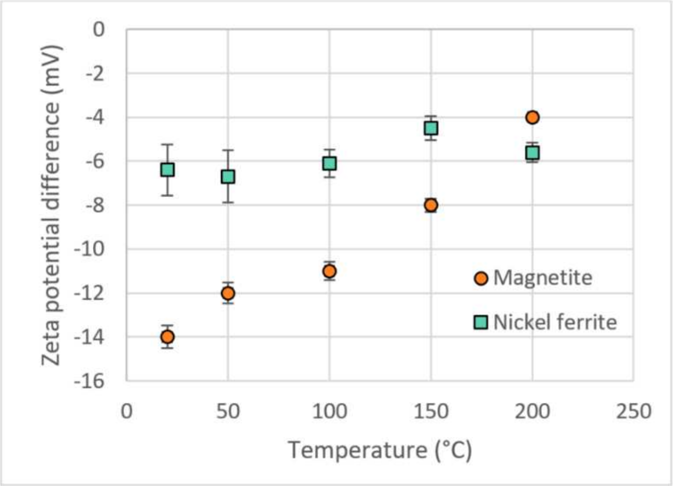

Figure 15. Variation with temperature of the difference in zeta potential between 1800 ppm and 1000 ppm of boron for magnetite and nickel ferrite ([Li]=3.5 ppm). (small column size)

When introducing boron as boric acid, a competition between the adsorption of borate ions and the decrease of the pH is occurring. As seen previously, while the adsorption of borates on the oxide surface leads to a decrease in the zeta potential value, the decrease of pH leads by definition to the presence of more positively charged species in the solution. Overall, the adsorption of borates has a predominant effect on the zeta potential value.

Contrary to when lithium hydroxide is introduced to boric acid solutions at [B] = 200 and 550 ppm, the introduction of boric acid at higher concentrations to lithium hydroxide solutions has no significant effect on the electrical resistance across the column (see Figure 16).

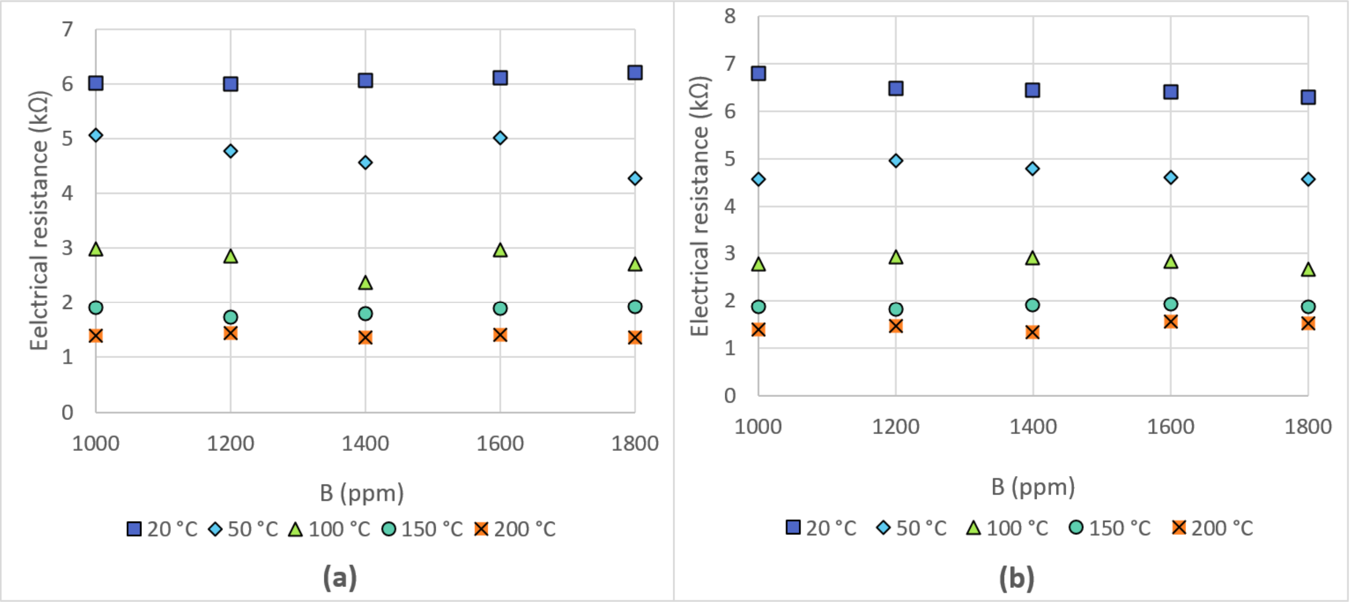

Figure 16. Influence of boron concentration on the electrical resistance of the (a) magnetite column (for [Li]=3.5 ppm) and (b) nickel ferrite column (for [Li]=3.5 ppm). (full page width)

As boron or lithium is introduced, a decrease in the electrical resistance may be expected due to higher ionic concentrations. However, boron at high concentrations does not seem to impact the value of the electrical resistance. This could be because at higher concentrations of lithium and boron the equilibrium $Li^{+} + B(OH)_4^{-} \rightleftharpoons LiB(OH)_4$ $(equation\ 17)$ is pushed towards the right hand side, forming neutral $LiB(OH)_4$.

Conclusion

This study presents values of zeta potential for commercial magnetite and synthesized nickel ferrite for twelve boron/lithium coordinations, representative of an operating cycle of the primary system of a PWR. The effects of the temperature, the pH, and the boron and lithium concentrations on the zeta potential were studied. Temperature as well as boric acid and lithium hydroxide concentrations were found to have a significant influence on the value of the zeta potential of the two oxides, typical of primary system corrosion products. The adsorption of borate ions on the surface of colloidal particles [29] overcomes the effect of the decrease of the pH on the zeta potential value when introducing boric acid in the system. Lithium ions were found to be indifferent toward the surface of colloids [16] and, therefore, the decrease of the zeta potential due to the introduction of lithium hydroxide can be explained by the increase of the pH.

This is the first time zeta potential values of representative corrosion products of the primary system have been obtained for temperature above 70 °C. As no other study reproduces the conditions of the primary system of PWRs, comparisons are difficult. However, the same trends concerning the effects of temperature and of boron and lithium ions on the zeta potential values were observed by Barale [15,16].

This unique set of values now constitutes the basis for an extrapolation to obtain zeta potential values in the conditions of the primary circuit, waiting for other experimental campaigns of zeta potential determination above 240 °C. These extrapolated values will be implemented in a model to predict the deposition of colloidal corrosion products in PWRs for the OSCAR code [30], developed by the CEA. This deposition model couples the transport step and the deposition step, taking into account surface effects, quantified through the notion of zeta potential.

Declaration of competing interest

The authors declare that they have no known competing financial interests or personal relationships that could have appeared to influence the work reported in this paper.

Acknowledgments

The authors gratefully acknowledge Mr. Jason Gorham and Mr. Adon Briggs of the Department of Chemical Engineering of the University of New Brunswick for their help and assistance with the machining and operations of the test section for the high-temperature water loop, and Mr. Nich Leaukosol, a staff member of UNB Nuclear, the University of New Brunswick nuclear research group, for helpful discussion and assisting in the loop preparation. S. Hettiarachchi and Konsta Sipilä are thanked for constructive comments on procedure.

This work is performed thanks to the financial support of The CEA, EDF and Framatome, with contributions from the CANDU Owners Group and Canada’s Natural Sciences and Engineering Research Council.

References

[1] S. Anthoni, P. Ridoux, Origin of corrosion products in PWR primary circuits, in: Eurocorr 96, Nice, 1996.
[2] D.H. Lister, Understanding and mitigating corrosion in nuclear reactor systems, in: Nucl. Corros. Sci. Eng., Elsevier, 2012: pp. 57–74. https://doi.org/10.1533/9780857095343.1.57.
[3] L. Marchetti-Sillans, Corrosion généralisée des alliages à base nickel en milieu aqueux à haute température : Apport à la compréhension des mécanismes, PhD thesis, Ecole Nationale Supérieure des Mines de Saint-Etienne, 2007. https://tel.archives-ouvertes.fr/tel-00991918 (accessed February 3, 2021).
[4] S. Gardey, Etude de la corrosion généralisée des alliages 600, 690 et 800 en milieu primaire. Contribution à la compréhension des mécanismes, PhD thesis, Université Pierre et Marie Curie, Paris VI, 1998.
[5] F. Carrette, Relâchement des produits de corrosion des tubes en alliage 690 de générateur de vapeur du circuit primaire des réacteurs à eau pressurisée, PhD thesis, Toulouse, INPT, 2002. http://www.theses.fr/2002INPT014G (accessed February 3, 2021).
[6] P. Millett, PWR Primary Water Chemistry Guidelines, EPRI, Palo Alto, 1999.
[7] F. Dacquait, Corrosion product transfer in french PWRs during shutdown, in: Proc. Int. Conf. Water Chem. Nucl. React. Syst., Avignon, France, 2002: p. paper 113.
[8] D.A. Briddle, The nature and behavior of particulates in PWR primary coolant, EPRI, 1989.
[9] P. Frattini, Characteristics of corrosion products in the loop and VVER plant primary systems, EPRI, 1999.
[10] T. Wen, Corrosion products characterization and radiation field buildup with Li/B modified chemical condition for Maanshan nuclear power plant, in: Proc. 1998 JAIF Int. Conf. Water Chem. Nucl. Power Plants, Kashiwazaki, Niigata, Japan, 1998.
[11] A.A. Strasser, Primary water chemistry, fuel rod corrosion, and crud deposition in PWRs – a comparison of european and US plant performance, EPRI, 1996.
[12] H. Marteau, Paluel-3 – Cycle 16 - Mesures EMECC et filtrations au début et en fin d’arrêt pour rechargement - Impact de l’arrêt sur le transfert de contamination, Comissariat à l’Energie Atomique, 2009.

[13] N. Epstein, Particulate Fouling of Heat Transfer Surfaces: Mechanisms and Models, in: L.F. Melo, T.R. Bott, C.A. Bernardo (Eds.), Fouling Sci. Technol., Springer Netherlands, Dordrecht, 1988: pp. 143–164. https://doi.org/10.1007/978-94-009-2813-8_10.

[14] B. Derjaguin, A theory of interaction of particles in presence of electric double layers and the stability of lyophobe colloids and disperse systems, Prog. Surf. Sci. 43 (1993) 1–14.

[15] M. Barale, Study of colloidal particles behaviour in the PWR primary circuit conditions, PhD thesis, Université Paris 6, 2006.

[16] M. Barale, G. Lefèvre, F. Carrette, H. Catalette, M. Fédoroff, G. Cote, Effect of the adsorption of lithium and borate species on the zeta potential of particles of cobalt ferrite, nickel ferrite, and magnetite, J. Colloid Interface Sci. 328 (2008) 7.

[17] C. Cherpin, D. Lister, F. Dacquait, L. Liu, S. Weerakul, Magnetite (Fe3O4) and nickel ferrite (NiFe2O4) zeta potential measurements at high temperature: Part I - Design, materials and preliminary characterization of an apparatus implementing the streaming potential method, Colloids Surf. Physicochem. Eng. Asp. (2022) 128961. https://doi.org/10.1016/j.colsurfa.2022.128961.

[18] C. Cherpin, D. Lister, F. Dacquait, L. Liu, Study of the Solid-State Synthesis of Nickel Ferrite (NiFe2O4) by X-ray Diffraction (XRD), Scanning Electron Microscopy (SEM) and Raman Spectroscopy, Materials. 14 (2021) 2557. https://doi.org/10.3390/ma14102557.

[19] P. Jayaweera, S. Hettiarachchi, Method and apparatus for measuring ζ potential of a substance at high temperature, US5280250A, 1994. https://patents.google.com/patent/US5280250A/en?oq=US5280250 (accessed April 18, 2021).

[20] ASTM D-3082-15 Standard test method for boron in water, 2017.

[21] P. Jayaweera, S. Hettiarachchi, B.G. Pound, Identifying Prospective Antifouling Coatings for Venturis, Electric Power Research Institute, 1992.

[22] R.E. Mesmer, C.F. Baes, F.H. Sweeton, Acidity measurements at elevated temperatures. VI. Boric acid equilibriums, Inorg. Chem. 11 (1972) 537–543. https://doi.org/10.1021/ic50109a023.

[23] S. Sasidharanpillai, H. Arcis, L. Trevani, P.R. Tremaine, Triborate Formation Constants and Polyborate Speciation under Hydrothermal Conditions by Raman Spectroscopy using a Titanium/Sapphire Flow Cell, J. Phys. Chem. B. 123 (2019) 5147–5159. https://doi.org/10.1021/acs.jpcb.9b03062.

[24] J.P. Ferguson, H. Arcis, P.R. Tremaine, Thermodynamics of Polyborates under Hydrothermal Conditions: Formation Constants and Limiting Conductivities of Triborate and Diborate, J. Chem. Eng. Data. 64 (2019) 4430–4443. https://doi.org/10.1021/acs.jced.9b00496.

[25] G. Plancque, D. You, E. Blanchard, Role of chemistry in the phenomena occurring in nuclear power plants circuits, in: Int Conf Adv. Nucl. Power Plants, Nice, France, 2011.

[26] J. McElrath, Pressurized Water Reactor Primary Water Chemistry Guidelines, Electric Power Research Institute, 2014.

[27] J. Deshon, P. Frattini, Adsorption of boric acid on synthetic fuel crud oxides, EPRI, 2002.

[28] D. Peak, G.W. Luther, D.L. Sparks, ATR-FTIR spectroscopic studies of boric acid adsorption on hydrous ferric oxide, Geochim. Cosmochim. Acta. 67 (2003) 2551–2560. https://doi.org/10.1016/S0016-7037(03)00096-6.

[29] J. Deshon, P. Frattini, Adsorption of Ions on Zirconium Oxide Surfaces from Aqueous Solutions at High Temperatures, Electric Power Research Institute, 2003.

[30] F. Dacquait, J. Francescatto, G. Galassi, F. Broutin, M. Gherrab, D. You, T. Jobert, N. Engler, The OSCAR v1.4 code: a new dissolution-precipitation model to better simulate the corrosion product transfer in nuclear cooling systems, in: Proc. Nucl. Plant Chem. Conf., San Fransisco, USA, 2018.

All figure captions

Figure 1. (a) SEM picture of synthesized nickel-ferrite (b) Quartz-vial used for the solid state-synthesis (c) SEM picture of commercial magnetite. (one and a half page width)

Figure 2. Boron/lithium co-ordinations imposed in the system and PWR high-lithium chemistry envelope. (small column size)

Figure 3. Evolution with temperature of the zeta potential of magnetite for different boron/lithium co-ordinations. (full page width)

Figure 4. Evolution with temperature of the zeta potential of nickel ferrite for different boron/lithium co-ordinations. (full page width)

Figure 5. Evolution of the zeta potential value of magnetite with temperature and the linear regression through all data ([B]=1800 ppm [Li]=3.5 ppm). (small column size)

Figure 6. Influence of the temperature on the electrical resistance of the magnetite column for duplicate runs ([B]=1800 ppm and [Li]=3.5 ppm) (small column size)

Figure 7. Streaming potential as a function of the pressure drop across the packed bed for a column packed with 0.5 g of magnetite between 20 °C and 200 °C for [B]=200 ppm and [Li]=1.5 ppm. (One and a half page width)

Figure 8. Evolution of the pH_T with the temperature for [B]=1800 ppm and [Li]=3.5 ppm. (small column size)

Figure 9. Evolution of zeta potential with pH_T of systems with a given boron/lithium coordination (written as B/Li) for a magnetite packed column. (full page width)

Figure 10. Evolution of zeta potential with pH_T of systems with a given boron/lithium coordination (written as B/Li) for a nickel ferrite packed column. (full page width)

Figure 11. Effect of the lithium concentration on the zeta potential of magnetite for a fixed concentration of boron of (a) 200 ppm and (b) 550 ppm. (full page width).

Figure 12. Effect of the lithium concentration on the zeta potential of nickel ferrite for a fixed concentration of boron of (a) 200 ppm and (b) 550 ppm. (full page width).

Figure 13. Effect of the boron concentration on the zeta potential of (a) magnetite and (b) nickel ferrite for [Li]=3.5 ppm. (full page width).

Figure 14. Possible reactions for the adsorption of boric acid on a surface. (small column size)

Figure 15. Variation with temperature of the difference in zeta potential between 1800 ppm and 1000 ppm of boron for magnetite and nickel ferrite ([Li]=3.5 ppm). (small column size)

Figure 16. Influence of boron concentration on the electrical resistance of the (a) magnetite column (for [Li]=3.5 ppm) and (b) nickel ferrite column (for [Li]=3.5 ppm). (full page width)

All tables

B/Li co-ordination	20 °C	50 °C	100 °C	150 °C	200 °C
0/0.5	-6.7 ±0.5	-6.2 ±0.5	-3.6 ±0.3	-1.2 ±0.1	-0.9 ±0.1
200/0.6	-4.4 ±0.3	-2.9 ±0.2	-2.0 ±0.2	0.0 ±0.1	1.1 ±0.1
200/1.0	-5.2 ±0.4	-3.2 ±0.2	-2.4 ±0.2	-1.4 ±0.1	0.5 ±0.1
200/1.5	-5.4 ±0.4	-4.4 ±0.3	-3.5 ±0.3	-2.5 ±0.2	-0.9 ±0.1
550/1.5	-5.1 ±0.4	-4.8 ±0.4	-3.8 ±0.3	-2.8 ±0.2	0.2 ±0.1
550/2.0	-6.3 ±0.5	-5.2 ±0.3	-4.1 ±0.2	-3.2 ±0.2	0.0 ±0.1
550/3.2	-6.4 ±0.4	-5.5 ±0.4	-4.8 ±0.4	-4.0 ±0.3	-0.8 ±0.1
1000/3.5	-4.7 ±0.3	-3.9 ±0.3	-3.1 ±0.2	-1.6 ±0.1	1.0 ±0.1
1200/3.5	-7.1 ±0.5	-5.9 ±0.4	-4.0 ±0.3	-2.4 ±0.2	0.1 ±0.1
1400/3.5	-7.9 ±0.6	-6.4 ±0.5	-5.6 ±0.4	-4.0 ±0.3	-1.6 ±0.1
1600/3.5	-8.5 ±0.8	-7.7 ±0.6	-5.9 ±0.4	-4.5 ±0.3	-1.5 ±0.1
1800/3.5	-9.3 ±0.7	-8.8 ±0.7	-7.8 ±0.6	-6.4 ±0.5	-2.6 ±0.2

Table 1. Values of zeta potential (mV) obtained for magnetite for the different boron/lithium (expressed as B/Li) co-ordinations for temperatures ranging from 20 °C to 200 °C.

Temperature (°C)	Zeta potential value (mV)
210	-2.5 ±0.2
220	-1.9 ±0.1
230	-1.6 ±0.2
240	-1.3 ±0.1

Table 2. Values of zeta potential of magnetite for temperatures ranging from 210 °C to 240 °C ([B]=1800 ppm and [Li]=3.5 ppm)

B/Li co-ordination	20 °C	50 °C	100 °C	150 °C	200 °C
0/0.5	-9.9 ±0.7	-5.5 ±0.4	-5.2 ±0.4	-0.6 ±0.1	-0.3 ±0.1
200/0.6	-8.0 ±0.6	-5.0 ±0.5	-3.2 ±0.4	0.9 ±0.1	3.5 ±0.3
200/1.0	-10.5 ±0.3	-6.7 ±0.2	-4.0 ±0.2	-1.4 ±0.1	-0.5 ±0.1
200/1.5	-14.2 ±1.0	-12.0 ±1.0	-10.0 ±0.9	-8.5 ±0.6	-5.6 ±0.4
550/1.5	-4.6 ±0.3	-3.5 ±0.2	-2.0 ±0.3	-0.5 ±0.4	0.7 ±0.1
550/2.0	-6.1 ±0.2	-4.9 ±0.1	-3.7 ±0.4	-1.9 ±0.3	-0.1 ±0.1
550/3.2	-8.7 ±0.6	-7.5 ±0.6	-5.6 ±0.4	-3.7 ±0.4	-2.1 ±0.2
1000/3.5	-6.5 ±1.3	-5.2 ±1.3	-2.9 ±0.6	-1.6 ±0.6	1.5 ±0.6
1200/3.5	-7.0 ±1.3	-5.9 ±0.9	-3.7 ±0.8	-1.8 ±0.5	0.8 ±0.4

1400/3.5	-7.9 ±0.5	-6.5 ±0.5	-4.5 ±0.7	-2.5 ±0.8	0.0 ±0.8
1600/3.5	-9.3 ±0.7	-8 ±0.4	-6.4 ±0.5	-4.0 ±0.6	-2.3 ±0.2
1800/3.5	-13.0 ±0.9	-12.0 ±1.0	-9.1 ±0.7	-6.1 ±0.5	-4.2 ±0.3

Table 3. Values of zeta potential (mV) obtained for nickel ferrite for the different boron/lithium co-ordinations for temperatures ranging from 20 °C to 200 °C.

pH (25 °C)		This study	Barale	
		20 °C [B]=550 ppm +Li	25 °C [B]=500 ppm [KCl]=10^{-4} mol/kg	25 °C [B]=500 ppm [LiCl]=10^{-4} mol/kg
$NiFe_2O_4$	6.9	-4.6 ±0.3 mV	-2 mV	10 mV
	7.2	-6.1 ±0.2 mV	-5 mV	2 mV
	7.4	-8.7 ±0.7 mV	-9 mV	-2 mV
Fe_3O_4	6.9	-5.1 ±0.4 mV	-18 mV	-13 mV
	7.2	-6.3 ±0.5 mV	-25 mV	-20 mV
	7.4	-6.4 ±0.4 mV	-33 mV	-25 mV

Table 4. Comparison of zeta potential values extracted from Barale with those obtained in this work for nickel ferrite and magnetite particles.

B (ppm)	Li (ppm)	pH_{EPRI} [26] (25 °C)	$pH_{PhreeqCEA}$ (300 °C)
0	0,5	9.85	7.18
200	0,6	6.9	6.95
200	1	7.1	7.17
200	1,5	7.27	7.34
550	1,5	6.72	7.06
550	2	6.85	7.18
550	3,2	7.06	7.38
1000	3,5	6.65	7.21
1200	3,5	6.48	7.14
1400	3,5	6.33	7.07
1600	3,5	6.19	7.02
1800	3,5	6.07	6.97

Table 5. Values of the pH at 25 °C from the EPRI and the PhreeqCEA values for 300 °C at the corresponding B/Li co-ordinations

Zeta potential measurement of $NiFe_2O_4$ and Fe_3O_4 between 20 and 240 °C